Neurobiology of Stress 13 (2020) 100247

Contents lists available at ScienceDirect

Neurobiology of Stress

journal homepage: www.elsevier.com/locate/ynstr

BNST transient activity associates with approach behavior in a stressful environment and is modulated by the parabrachial nucleus

A.A. Jaramillo [a,b,c,d], K.M. Williford [a,c,d], C. Marshall [a,b,c,d], D.G. Winder [a,b,c,d,e,f,g,**], S. W. Centanni [a,b,c,d,*]

[a] Vanderbilt University School of Medicine, Nashville, TN, USA
[b] Dept. Mol. Phys. & Biophysics, Nashville, TN, USA
[c] Vanderbilt Brain Institute, Nashville, TN, USA
[d] Vanderbilt Center for Addiction Research, Nashville, TN, USA
[e] Vanderbilt Kennedy Center, Nashville, TN, USA
[f] Department of Psychiatry & Behavioral Sciences, Nashville, TN, USA
[g] Department of Pharmacology, Nashville, TN, USA

ARTICLE INFO

Keywords:
BNST
PBN
PKCδ
Approach
Stress
Anxiety

ABSTRACT

Studies demonstrate a role for the bed nucleus of the stria terminalis (BNST) in modulating affective behavior and stress-reward integration. To explore the dynamic nature of *in vivo* BNST activity associated with anxiety-like behavior in a stress-inducing context, we utilized fiber photometry and detected BNST calcium transients in mice during the novelty-suppressed feeding task (NSFT). Phasic BNST activity emerged time-locked to novel object or food pellet approach during NSFT. The parabrachial nucleus (PBN) has a large input to the BNST and is thought to function as a danger signal, in arousal responses and in feeding behavior. To explore a potential role for the PBN as a contributor to BNST activity in NSFT, we investigated whether chemogenetic regulation of PBN activity altered the dynamic BNST response synchronized to NSFT approach behavior. We found that activation of the hM3D(G_q) DREADD in the PBN enhanced the observed transient signal in the BNST synchronized to the consummatory food approach, and was associated at the behavioral level with increased latency to consume food. Because the PBN has multiple efferent pathways, we next used a transsynaptic anterograde AAV-based strategy to express hM3D(G_q) specifically in PBN-innervated BNST ($BNST^{PBN}$) neurons in male and female mice. Activation of hM3D(G_q) in these $BNST^{PBN}$ neurons increased latency to consume food in female, but not male mice. To further explore the population of BNST neurons contributing to phasic BNST activity associated with NSFT, we turned to PKCδ neurons in BNST. BNST(PKCδ) neurons are implicated in stress and food-related behavior, and we previously found that the expression of this kinase is regulated in the BNST by stress in a sex-dependent manner. Here, we demonstrate close apposition of CGRP, a marker of PBN terminals, adjacent to BNST(PKCδ) cells. Finally, we find that PKCδ-expressing BNST cells exhibit a large transient signal synchronized to the consummatory food approach similar to that seen with bulk BNST activity measures. Taken together these data demonstrate phasic BNST activity at a global and cell-specific level that is driven in part by PBN activity at the time of NSFT consummatory approach behavior.

1. Introduction

Psychiatric disorders can involve maladaptive responses to stressors in contexts that require the selection of an approach or avoidance behavior (Miller, 1944; Shin and Liberzon, 2010). The bed nucleus of the stria terminalis (BNST), a component of the extended amygdala, is an evolutionarily conserved basal forebrain region that modulates key midbrain and brainstem response centers during stress (Adhikari, 2014; Avery et al., 2016; Avery et al., 2014; Dong et al., 2001; Flook et al., 2020; Lebow and Chen, 2016; Novais et al., 2017; Kirlic et al., 2017; Walker et al., 2003). Previous studies that manipulate the BNST demonstrate a necessary role for the structure in regulating stress

* Corresponding author. 865 Light Hall, 2215 Garland Avenue, Nashville, TN, 37232, USA.
** Corresponding author. 875A Light Hall, 2215 Garland Avenue, Nashville, TN, 37232, USA.
E-mail addresses: danny.winder@vanderbilt.edu (D.G. Winder), samuel.centanni@vanderbilt.edu (S.W. Centanni).

https://doi.org/10.1016/j.ynstr.2020.100247
Received 30 April 2020; Received in revised form 25 June 2020; Accepted 20 July 2020
Available online 1 August 2020

responses (Walker et al., 2003; Wenzel et al., 2011), and recent endoscopic imaging techniques demonstrate unique BNST responses during a variety of anxiety- and fear-inducing contexts (Bjorni et al., 2020; Giardino et al., 2018; Harris et al., 2018). Furthermore subregion, cell- and projection-specific BNST manipulations reveal a complex and sexually dimorphic role of the BNST in various stress-like behaviors (Giardino et al., 2018; Lebow and Chen, 2016; Walker et al., 2003). Thus, investigating BNST activity and the circuits that govern it during stressful situations is critical for insight into maladaptive stress responses.

To determine patterns of BNST activity *in vivo* during an anxiety-inducing stress situation, the present study used fiber photometry to visualize bulk and cell-specific calcium signals during the novelty-suppressed feeding task (NSFT), a pharmacologically-validated test for assessing aspects of negative affective state in mice (Bodnoff et al., 1988; Britton and Britton, 1981; Corr, 2013; Cryan and Sweeney, 2011; Goode and Maren, 2017; Kirlic et al., 2017). While we previously showed BNST recruitment in NSFT (Centanni et al., 2019), those findings measured static changes in BNST activity following the anxiety-like behavior. Here we investigate the dynamic temporal nature of BNST activity throughout the stress-inducing NSFT which measures latency to feed on a centrally-located pellet in an open field box. Given the food-restricted state and innate avoidance of the center, NSFT provides a stress-like context. We begin to tease apart the relationship between BNST activity and NSFT-induced anxiety-like behavior by moving the food location and replacing the food with a non-appetitive object. Next, to begin investigating determinants of temporal BNST activity we looked upstream by focusing on an afferent input to the BNST during NSFT *in vivo*. Given the substantial anatomical input from the parabrachial nucleus (PBN) to the BNST, neurochemical and electrophysiological evidence of PBN somatic innervation of BNST neurons (Campos et al., 2017; Carter et al., 2013; Chen et al., 2018; Fetterly et al., 2019; Flavin et al., 2014), and the role of this region in arousal and food-related behavior in a stress-like state (Carter et al., 2013; Palmiter, 2018), we explored the impact of PBN manipulation on BNST activity. Furthermore, to dissect the role of PBN-BNST circuitry regulating NSFT behavior, we focused postsynaptically by utilizing an anterograde transneuronal viral approach (Centanni et al., 2019; Zingg et al., 2017; Zingg et al., 2020) to selectively excite BNST neurons innervated by the PBN ($BNST^{PBN}$). Moreover, we and others have demonstrated stress-induced changes in a distinct BNST subpopulation expressing protein kinase C δ (PKCδ), implicated in BNST-mediated response to stress (Fetterly et al., 2019). To investigate the neuron heterogeneity within the measured bulk temporal BNST activity, we used immunohistochemistry to visualize PBN innervation onto PKCδ-expressing neurons in the BNST and then detected isolated calcium activity in PKCδ-expressing BNST neurons during NSFT.

In summary these data demonstrate bulk and PKCδ neuron-specific transient signals in the BNST associated with food approach during NSFT. Additionally, we find a PBN-induced delay to initiate the consummatory approach behavior synchronized to a potentiation of the BNST transient signal. $BNST^{PBN}$ hM3D(G_q) activation was associated with increased anxiety-like behavior in female but not male mice suggesting a potential sex-specific aspect of this pathway. On this basis, these data highlight a role for the PBN→BNST circuit in anxiety-like behavior by integrating activity and behavior in the BNST.

2. Material and methods

2.1. Animals

Mice were single (Experiments 1–3) or group housed (Experiment 2) with water and food available *ad lib* in the home cage until the test day. The colony room was maintained on a 12-h light/dark cycle (lights on at 06:00 under controlled temperature (20–25 °C) and humidity (30–50%) levels. All experiments were conducted during the light phase. Animals were under continuous care and monitoring by veterinary staff from the Vanderbilt Division of Animal Care. All procedures were carried out in accordance with the NIH Guide to Care and Use of Laboratory Animals and institutional guidelines and approved by the Institutional Animal Care and Use Committee at Vanderbilt University.

2.2. Viral injections/stereotaxic surgery

Adult mice (>8 weeks) were anesthetized with isoflurane (initial dose = 3%; maintenance dose = 1.5%) and surgery was performed using a stereotax (Leica). Coordinates from bregma were used to target the BNST (AP = 0.14, ML±0.88, DV = −4.18, 15.03° angle) and the PBN (AP = −5.34, ML±1.31, DV = −3.37, 15.03° angle). For viral injections, 300 nL (40 nL/min) were infused and the needle remained in place for an additional 5-min before withdrawal. For fiber optic implants a gel etchant (Kerr) was applied, ferrule was lowered through the craniotomy, and cured following application of the primer (Optibond), adhesive (Optibond), and Herculite Unidose Enamel (KRVl). Mice were treated with Alloxate (2.5 mg/kg, S.C.) for 72-hr after surgery and allowed to recover for at least 1 week before further experimentation.

2.3. Behavioral testing

The 3-day novelty-suppressed feeding task (NSFT) was performed as previously described (Britton and Britton, 1981; Centanni et al., 2019; Holleran et al., 2016). In brief, mice were food restricted in their home cage with no food for 48-hr except for 2-hr access to food pellets (approximately 2 pellets = 7 g) at the 22–24hr before testing. Mice were weighed before and after restriction to ensure weight loss was similar across all groups. After 48-hr of restriction (testing day) mice were acclimated to the testing room for at least 1-hr. For the test, a single food pellet was placed at the center of a brightly-lit (300 lux) 50 × 50 cm arena with fresh home cage bedding. A new pellet was used and bedding was refreshed for each test. At the time of testing a mouse was placed in a corner of the arena with an overhead video camera. ANYMaze software (Stoelting Co) was used to track all food approaches and the time of the first bite. Following the first bite (final, consummatory food approach) mice were immediately removed from the arena and returned to the home cage with the pellet from the test or a fresh pellet which was then weighed after 10 min. Mice that did not eat within the first 20-min of the test and/or post-test were omitted from analysis. Following the test, the mice were returned to *ad lib* access to chow.

2.4. Fiber photometry system

Bulk BNST GCaMP recordings were acquired using the ChiSquare 2–202 dual-probe system (ChiSquare Bioimaging; Supplemental Fig. 1a) as previously described (Cui et al., 2014; Harris et al., 2018). Briefly, fiber optic ferrules were made in house: a 0.22 NA 300 μm core single mode (Thorlabs) was cut with an Ideal DualScribe Wedge Tip Carbide Scribe (Fiber Optic Center) and cured at 45 °C overnight into a ferrule (Thorlabs) with Epo-Tek epoxy (Fiber Optic Center), and polished with Ferrule Polishing Disc (Thorlabs) on finer aluminum oxide lapping sheets (5, 3, 1, 0.1 μm; Thorlabs). Both sides were visually inspected for aberrations and not used if light output from the connected fiber tip was <90% of the power output from the patch cord alone. Once implanted onto the mouse skull the ferrule was tethered to the fiber photometry system by a flexible patch cord allowing the mouse to be freely moving. Blue light from a 473 nm picosecond-pulsed laser (at 50 MHz; pulse width ~80 ps FWHM) was delivered to the tissue through the single mode fiber. Fluorescence emission from the tissue was collected by the multimode fiber. The emitted photons collected through the multimode fiber passed through a band-pass filter (FF01-550/88; Semrock) to a single-photon detector. Photons were recorded by the time-correlated single photon counting module (SPC-130EM; Becker and Hickl). A fluorescence intensity trace was obtained by plotting the number of

photons recorded in 20 ms intervals against time. Fluorescence decay kinetics were used to confirm *in vivo* GCaMP expression.

BNST PKCδ^{CRE} GCaMP7f recordings were acquired by tethering freely moving mice implanted with an optical fiber ferrule (MFC_400/430–0.57_4 mm_MF2.5_FLT Mono) to a Tucker-Davis Technologies fiber photometry detection system (Supplemental Fig. 1b), consisting of a RZ5P processor and Synapse custom software and optical components (Doric Lenses; ThorLabs). LEDs (470 nm blue light and 405 nm violet light) were relayed through a filtered fluorescence minicube at spectral bandwidths, of 460–495 nm and 405 nm, and delivered to the tissue through the 400 μm single mode fiber. Power output for the primary 470 nm wavelength at the tip of the fiberoptic cable was measured at ~25-30μW. Single emissions were detected using a femtowatt photoreceiver with a lensed fiber cable adapter and filtered at 500–550 nm 470 nm and 405 nm wavelengths were modulated at frequencies of 210–220 and 330 Hz, respectively, and power output maintained at 20 mA with a DC offset of 3 mA for both light sources. All signals were acquired at 1 kHz and lowpass filtered at 3 Hz. Linear regression was utilized to correct for the bleaching of signal for the duration of each recording, using the slope of the 405 nm signal fitted against the 470 nm signal.

Final measures for the change in activity of the recorded cells across all tasks was made by running the collected photometry data through a custom analysis algorithm in MATLAB. The analysis normalized the photon counts to $\Delta F/F_0$ values to correct for artifact deviations within each individual animal. A Z-Score transformation was then computed to compare across animals and compensate for the innate difference in dynamic range of individual GCaMP signals. Fiber photometry recordings began upon receipt of a transistor-transistor logic pulse from ANY-Maze to precisely time-lock the BNST GCaMP signal to behavior and normalized -5s to -3s prior to approach behavior.

2.5. Ultrasonic vocalizations

Ultrasonic Vocalization (USVs) were recorded in Experiment 2 during NSFT using Avisoft software Version 4.2 and an ultrasonic microphone (Avisoft Bioacoustics) 60 cm above the NSFT open field arena. USV data were analyzed with the DeepSqueak 2.0 algorithm (Coffey et al., 2019) in MATLAB.

2.6. Experimental procedures

2.6.1. Experiment 1: Examination of BNST in vivo activity during NSFT

We focused initially on females due to our previous studies indicating that female C57BL/6J mice exhibit substantial alterations in NSFT behavior after forced abstinence from chronic alcohol exposure (Centanni et al., 2019). Prior to the start of testing, C57BL/6J female mice (n = 6; Jackson Laboratory) received a unilateral injection of the calcium sensor AAV5-hSyn-GCaMP6f-WPRE (Addgene) and a fiberoptic implant in the BNST (Fig. 1a). Following recovery from surgery mice were habituated to headpost manipulations (e.g., cleaning) and to the fiber optic cable for fiber photometry recordings (Supplemental Fig. 1a) for 3 days. Next, female mice underwent the 3-day NSFT paradigm (Fig. 1b) and on test day were habituated to the fiber optic cable >30s to obtain a stable baseline GCaMP signal prior to testing. GCaMP recordings were obtained throughout the entire test. To investigate if BNST activity and behavior would be affected by different anxiety-like states in NSFT, female mice were food restricted and tested with the following modifications to the NSFT paradigm: food pellet was relocated from center to a corner and food pellet was replaced with a novel object (i.e., battery), measuring context- and appetitive-associated stress respectively (Fig. 1g and e insets). An additional cohort (n = 4/group) of non-surgerized C57BL/6J female mice were added to the behavioral data from the modified NSFT test (as denoted by grey symbols, Fig. 1k–m) to control for the effects of surgery and viral expression on behavior. To control for false positives in GCaMP detection a separate group of C57BL/6J female mice (n = 2) received unilateral injections of a calcium independent green fluorophore AAV5-hSyn-eGFP (Addgene) in the BNST, and were tested with the non-modified NSFT protocol (food pellet in center).

2.6.2. Experiment 2: Effects of excitatory PBN activation on BNST in vivo activity during NSFT

CGRP (gene name *Calca*) is a protein specifically expressed on PBN inputs to the BNST (Carter et al., 2013; Chen et al., 2018; Fetterly et al., 2019; Flavin et al., 2014; Wang et al., 2019), thereby *Calca*^{CRE} female and male mice bred and genotyped in house (Mccoy et al., 2013) were used. Female and male mice received a unilateral injection of the calcium sensor AAV9-hSyn-jGCaMP7f-WPRE (Addgene) and a fiberoptic implant in the BNST and concurrent bilateral injections of the excitatory CRE-dependent DREADD AAV5-hSyn-DIO-hM3D(G_q)-mCherry (hM3D [G_q]; UNC Vector Core: 9 females, 6 males) or CRE-dependent control fluorophore AAV5-hSyn-DIO-mCherry (mCherry; Addgene; 10 females, 6 males) in the PBN (Fig. 1a–c). Mice with inefficient viral expression (1 female and 1 male) and head post attrition (2 females and 3 males) were not included in the hM3D(G_q) fiber photometry data but were included in the behavior data when appropriate (i.e., saline). In the mCherry group, mice with inefficient viral expression (1 female) and mice with head post attrition (6 females and 1 male) were not included in mCherry photometry data. Following recovery from surgery, female and male mice underwent the same 3-day NSFT protocol as in Experiment 1 (Fig. 1b). On test day, mice received CNO (3 mg/kg I.P.) in their home cage 30-min prior to the fiber photometry recording (Supplemental Fig. 1a) and in addition USVs were recorded during the test (Fig. 2a).

2.6.3. Experiment 3: Examination of BNST^{PBN} activation on NSFT

C57BL/6J female (n = 9) and male (n = 7) mice (Jackson Laboratory) received bilateral injections of the transsynaptic anterograde AAV1-hSyn-CRE (Addgene (Zingg et al., 2017; Zingg et al., 2020); in the PBN combined with the excitatory CRE-dependent DREADD AAV5-hSyn-DIO-hM3D(G_q)-mCherry (Centanni et al., 2019) in the BNST. Mice with inefficient viral expression (3 female) and mice that did not consume food post-NSFT (1 female) were not included in the behavioral data. The same NSFT testing protocol (Fig. 1b) and CNO pretreatment as in Experiment 2 was used (Fig. 3a).

2.6.4. Experiment 4: Examination of PBN innervation onto PKCδ expressing BNST cells and PKCδ-specific BNST in vivo activity during NSFT

Tissue from PKCδ^{CRE} female (n = 8) and male (n = 2) mice (bred and genotyped in house, transgenic mouse line provided by Mutant Mouse Resource and Research Centers (MMRRC) at UC-Davis (# 011559-UCD, STOCK Tg(Prkcd-glc-1/CFP,-CRE)EH124Gsat/Mmucd)) was processed with immunohistochemistry and analyzed for PKCδ and CGRP expression in BNST cells. A separate group of PKCδ^{CRE} female (n = 5) and male (n = 3) mice received a unilateral injection of the CRE-dependent calcium sensor AAV9-hSyn-FLEX-jGCaMP7f-WPRE (Addgene) and a fiberoptic implant in the BNST (Fig. 4c) for fiber photometry recordings (Supplemental Fig. 1b). Mice with inefficient GCaMP expression (1 male) were not included in the data. Following recovery from surgery, the same NSFT testing protocol (Fig. 1b) as in Experiment 1 was used (Fig. 4c).

2.7. Tissue preparation for viral vector confirmation

Mice were deeply anesthetized using isoflurane, transcardially perfused with ice-cold phosphate buffered saline (PBS) followed by 4% paraformaldehyde (PFA) in PBS. Brains were submerged in 4% PFA for 24-hr at 4 °C and cryoprotected in 30% sucrose in PBS for a minimum of 5 days. Coronal sections were cut on a cryostat (Leica, CM3050S) in Optimal Cutting Temperature solution (VWR) at a thickness of 40 μm and stored in PBS at 4 °C. GCaMP and hM3D(G_q)-mCherry or mCherry-Control expression was confirmed by immunofluorescence with a

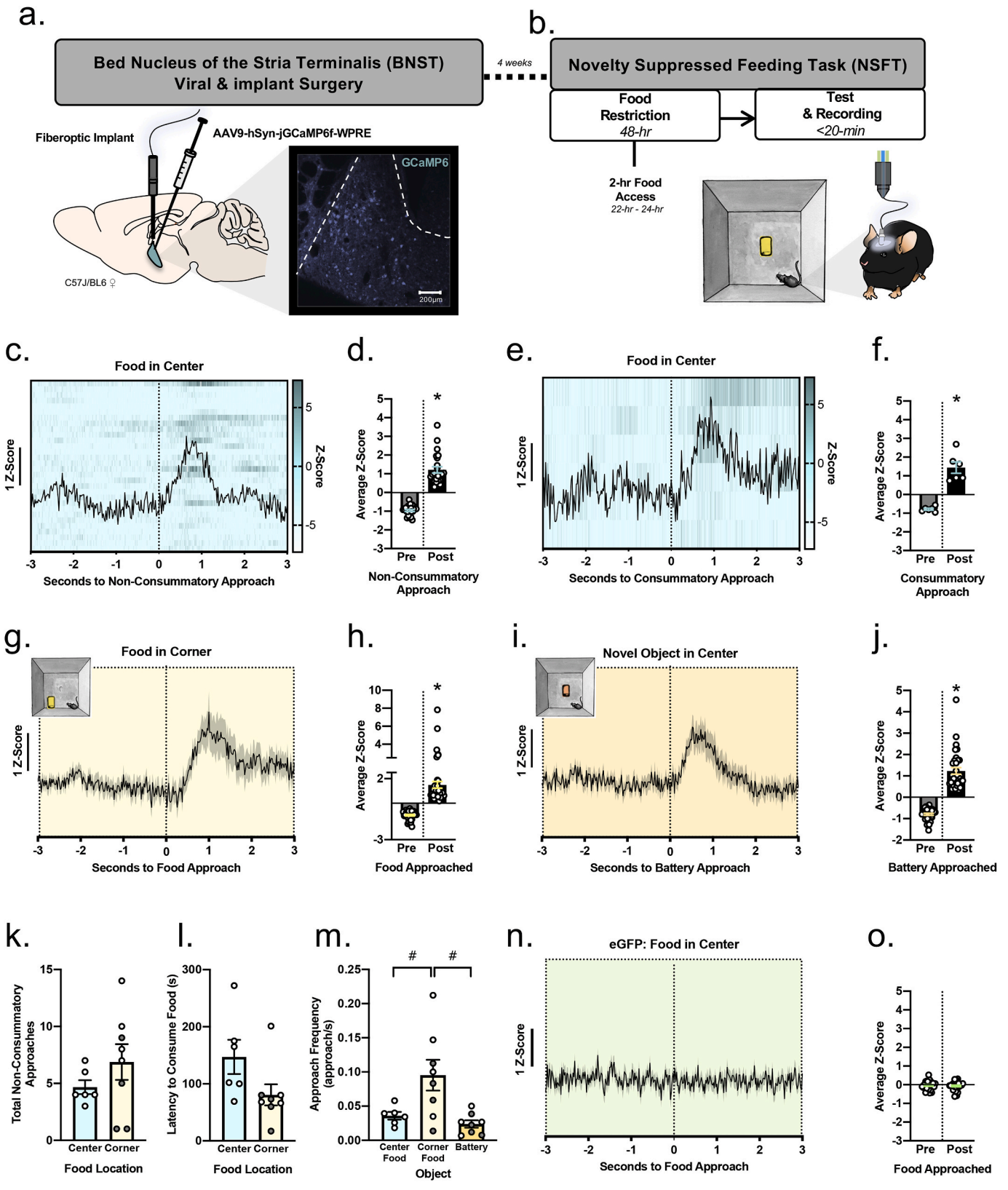

(caption on next page)

Fig. 1. Temporal BNST phasic GCaMP transients emerge during the time of approach in a Novelty-Suppressed Feeding Task. **a)** Representative BNST GCaMP6f autofluorescence following unilateral GCaMP6f infusion & fiber optic implantation in the BNST of C57BL/6J female mice. **b)** Timeline of the novelty-suppressed feeding task (NSFT) paradigm to measure center food approaches and latency to initiate a consummatory approach. **c)** Mean ± S.E.M of BNST GCaMP6f Z-Scores at the time of approaching food (i.e., food is not obtained) shows a transient signal. **d)** Mean ± S.E.M of the individual GCaMP6f Z-Score averages is significantly increased after the time of a non-consummatory approach bout ($p < 0.0001$). **e)** Mean ± S.E.M of BNST GCaMP6f Z-Scores at the time of the consummatory food approach shows a transient signal. **f)** Mean ± S.E.M of individual GCaMP6f Z-Score averages is significantly increased after the time of the consummatory approach ($p = 0.0015$). **g)** Mean ± S.E.M of BNST GCaMP6f Z-Scores at the time of corner food approach during the modified NSFT (inset) shows a transient signal. **h)** Mean ± S.E.M of the individual GCaMP6f Z-Score averages is significantly increased after the time of a corner food approach ($p < 0.0001$). **i)** Mean ± S.E.M of BNST GCaMP6f Z-Scores at the time of a novel object approach in the modified NSFT (i.e., battery; inset) shows a transient signal. **j)** Mean ± S.E.M of the individual GCaMP6f Z-Score averages is significantly increased after the time of a battery approach ($p = 0.0205$). **k)** Mean ± S.E.M of the total non-consummatory food approaches and **l)** latency for the consummatory approach were similar in the NSFT (center food) and modified NSFT (corner food). **m)** Mean ± S.E.M approach frequency in NSFT is increased toward the corner-located food relative to center-located food ($p = 0.0344$) and center-located novel object ($p = 0.0059$). **n)** Mean ± S.E.M of BNST eGFP Z-Scores at the time of food approach shows no transient signal. **o)** Mean ± S.E.M of the individual eGFP Z-Score averages is similar post time of a food approach. Overlaid heatmaps display rows of individual BNST GCaMP6f Z-Scores across columns of time with darker colors indicating higher Z-Scores. *Significant difference from pre approach (paired *t*-test), #Significant from corner food (One way-ANOVA, Tukey's), $p \leqq 0.05$. . (For interpretation of the references to color in this figure legend, the reader is referred to the Web version of this article.)

Keyence BZ-X710 microscope. To visualize CRE expression sections were incubated in mouse anti-CRE primary antibody (1:1000; MilliporeSigma) for 48-hr at room temperature, washed in PBS, and incubated in Cy5 donkey anti-mouse secondary antibody (1:500; Jackson ImmunoResearch) in 0.1% Triton X-100 in PBS for 24-hr at 4 °C. To visualize PKCδ and CGRP colocalization sections were incubated in goat anti-CGRP primary antibody (1:400; Abcam) for 48-hr at 4 °C followed by mouse anti-PKCδ primary antibody (1:1000; BD Biosciences) for 24-hr at 4 °C, washed in PBS, and incubated in Cy3 donkey anti-goat (1:500, Jackson ImmunoResearch) and Cy5 donkey anti-mouse (1:500) secondary antibodies for 24-hr at 4 °C. To visualize PKCδ and GCaMP sections were instead incubated in Cy3 donkey anti-mouse secondary antibody (1:500; Jackson ImmunoResearch). Sections were washed with PBS and mounted on Fisher frost-plus slides. For viral placement confirmation representative images were taken using a Nikon Multi Excitation TIRF microscope with a 10x/0.45 N.A. and 20x/0.75 N.A. Plan-Apochromat objective lenses. Only mice with accurate viral and implant injections were included in the analysis and data presentation. CGRP + PKCδ slices were imaged at 20x magnification on a Zeiss LSM 880 confocal microscope and analyzed using ImageJ software (NIH), with the same brightness and contrast settings applied across all images.

2.8. Drugs

Sterile saline or 3 mg/kg Clozapine-N-oxide (CNO, MilliporeSigma) diluted in diH_20 were delivered I.P.

2.9. Data analysis

Data is represented as mean ± S.E.M and all statistics were run using Prism 7 (GraphPad). Differences between groups were assessed using *t*-tests, One-way ANOVAs, Two-way ANOVAs, and Tukey's post hoc test, with significance set at $p \leqq 0.05$.

3. Results

3.1. Experiment 1: phasic BNST calcium signal associated with NSFT approach behavior

Bulk calcium recordings in the BNST were measured during NSFT to impute *in vivo* BNST neuronal activity during anxiety-like behavior. C57BL/6J female mice received a unilateral injection of the calcium indicator AAV5-hSyn-GCaMP6f-WPRE and were implanted with a fiber optic in the BNST (Fig. 1a.). Following recovery from surgery, BNST calcium activity was recorded (Supplemental Fig. 1a) during NSFT and latency to feed was measured (Fig. 1b). A clear BNST transient signal was observed at the time of non-consummatory chow approaches (Fig. 1c) and the consummatory approach that resulted in feeding (Fig. 1f), demonstrated by a significant increase in amplitude measured by average Z-Score pre-versus post-approach (Fig. 1d, [$t_{23} = 14.66$, $p < 0.0001$]; Fig. 1e, [$t_5 = 6.256$, $p = 0.0015$]).

Next, we sought to tease apart whether the food location in NSFT was the determinant of the BNST transient detected at the time of approach. Thereby prior to testing the food pellet was relocated from the center to a corner in the NSFT box (Fig. 1g inset). A clear BNST transient at the time of approach towards the corner food was detected (Fig. 1g) demonstrated by the significant increase of the average Z-Score pre-versus post-approach (Fig. 1h, [$t_{32} = 9.023$, $p < 0.0001$]). Next, to investigate whether the food was the determinant of the BNST transient detected at the time of food approach, a novel object (battery of similar size as the food) replaced the food pellet prior to testing. A clear BNST transient was detected at the time of approach (Fig. 1i) shown by the significant increase in amplitude measured by average Z-Score pre-versus post-approach (Fig. 1j, [$t_{32} = 12.72$, $p < 0.0001$]). Comparison of the behavioral data from the modified NSFT demonstrate no effect of food location (center versus corner) on total non-consummatory approach bouts (Fig. 1k, [$t_{12} = 1.156$, $p = 0.2703$]). There was a trend towards increased latency to consume the center-located food compared to corner-located food (Fig. 1l, [$t_{12} = 1.980$, $p = 0.0710$]). One-way ANOVA comparing approach frequency shows a significant increase in frequency of corner-located food (Fig. 1m, [$F_{(2,19)} = 7.011$, $p = 0.0108$]) relative to center-located food ($p = 0.0344$) and to the novel object ($p = 0.0059$). To control for the effects of surgery and GCaMP viral expression on behavior an additional cohort of non-surgerized C57BL/6J female mice was tested (denoted by grey symbols in Fig. 1k–m). No differences were observed therefore the behavioral data was combined with the GCaMP fiber photometry C57BL/6J female mice group to increase statistical power. Next, to validate the fidelity of the detected BNST GCaMP transients, a separate cohort of C57BL/6J female mice were injected with AAV5-hSyn-eGFP in the BNST (Fig. 1n inset) implanted with a fiber optic and tested in NSFT. No significant change in BNST eGFP signal was observed in NSFT at the time of food approach bouts measured by average Z-Score pre-versus post-approach, (Fig. 1n-o, [$t_{28} = 0.6482$, $p = 0.5222$]). Together these data reveal phasic BNST GCaMP transients at the time of a center and corner food approach and a center-located novel object approach.

3.2. Experiment 2: PBN enhances the phasic BNST calcium signal associated with a delay in NSFT consummatory approach behavior

To assess circuit inputs that regulate the BNST transients we focused upstream on the PBN due to its role in modulating alert responses (Campos et al., 2017; Palmiter, 2018) and our recent findings that show a PBN-induced effect on the BNST following stress (Fetterly et al., 2019). Given that the PBN sends calcitonin gene-related peptide (CGRP) inputs to the BNST (Carter et al., 2013; Chen et al., 2018; Fetterly et al., 2019; Flavin et al., 2014; Wang et al., 2019), which may in part be differentially regulated in males and females (Fetterly et al., 2019), *Calca*^{CRE}

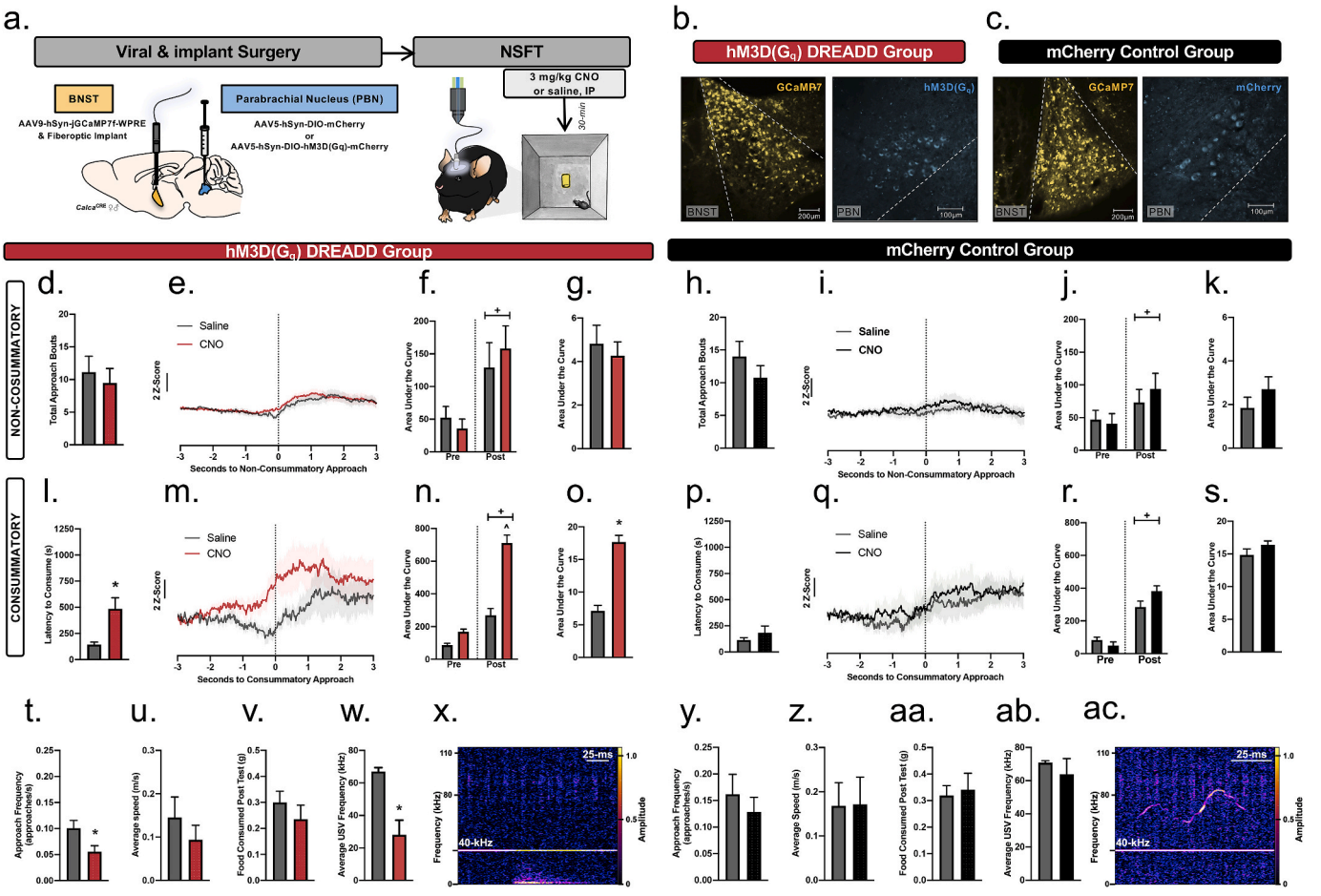

Fig. 2. Global PBN activation increased phasic BNST transient amplitude and latency to feed during NSFT. **a)** Experimental paradigm demonstrates viral unilateral GCaMP7f infusion & fiber optic implantation in the BNST with concurrent bilateral infusions of CRE-dependent hM3D(G_q) or mCherry in the PBN of *Calca*^{CRE} female and male mice. Following recovery from surgery mice were tested on the NSFT paradigm with a 30-min pretreatment of CNO (3 mg/kg, IP) or saline. **b**) Representative image of the hM3D(G_q) group showing GCaMP7 and hM3D(G_q) autofluorescence in the BNST and PBN respectively. **c)** Representative image of the mCherry group showing GCaMP7 and mCherry fluorophore autofluorescence in the BNST and PBN respectively. **d)** In the hM3D(G_q) group the mean ± S.E.M. of total non-consummatory food approaches is similar between saline and CNO treatment. **e)** Mean ± S.E.M of BNST GCaMP7f Z-Scores during non-consummatory food approaches shows a transient signal, **f**) with an increase in the mean ± S.E.M area under the curve (AUC) post the time of non-consummatory food approach with saline and CNO treatment in the hM3D(G_q) group ($p = 0.0004$). **g)** Total mean ± S.E.M AUC of BNST GCaMP7f Z-Score signal is similar throughout non-consummatory food approaches with saline and CNO treatment in the hM3D(G_q) group. **h**) In the mCherry group the mean ± S.E.M. of total non-consummatory food approaches is similar between saline and CNO treatment. **i)** Mean ± S.E.M of BNST GCaMP7f Z-Scores during non-consummatory food approaches shows a transient signal, **j**) with an increase in the mean ± S.E.M area under the curve (AUC) post the time of non-consummatory food approach with saline and CNO treatment in the mCherry group ($p = 0.0353$). **k)** Total mean ± S.E.M AUC of BNST GCaMP7f Z-Score signal is similar throughout non-consummatory food approaches with saline and CNO treatment in the mCherry group. **l)** In the hM3D(G_q) group, CNO treatment (3 mg/kg, IP) increased mean ± S.E.M. latency to initiate food consumption ($p = 0.046$). **m**) During the time of the consummatory approach the mean ± S.E.M of BNST GCaMP7f Z-Scores shows a transient signal **n**) with an increase in the mean ± S.E.M AUC post the time of the consummatory approach with saline and CNO treatment in the hM3D(G_q) group. CNO potentiated the increase in mean ± S.E.M AUC of BNST GCaMP7f Z-Score signal post the initiation of the consummatory approach ($p < 0.0001$) **o)** and the total mean ± S.E.M AUC ($p = 0.0038$) throughout the consummatory approach in the hM3D(G_q) group. **p)** In the mCherry group, mean ± S.E.M. latency to initiate food consumption was similar with saline and CNO. **q**) In the mCherry group, during the time of the consummatory approach the mean ± S.E.M of BNST GCaMP7f Z-Scores shows a transient signal **r**) as there is an increase in the mean ± S.E.M AUC post the time of the consummatory approach with saline and CNO treatment. **s**) The total mean ± S.E.M AUC throughout the consummatory approach was similar with saline and CNO treatment in the mChery group. **t)** Mean ± S.E.M approach frequency significantly decreased with CNO treatment in the hM3D(G_q) group ($p = 0.0226$). **u)** Mean ± S.E.M speed and **v)** total food consumed was similar with saline and CNO in the hM3D(G_q) group. **w**) CNO decreased mean ± S.E.M USV frequency (kHz) in the hM3D(G_q) group ($p = 0.0093$). **x**) Sonogram showing a representative low frequency (<40 kHz, horizontal yellow line) ultrasonic vocalization (USV) with CNO treatment in the hM3D(G_q) group. **y**) In the mCherry group the mean ± S.E.M approach frequency, **z)** speed, **aa**) total food consumed, and **ab**) USV frequency was similar with saline and CNO. **ac**) Sonogram showing a representative high frequency (>40 kHz, horizontal yellow line) USV following CNO in the mCherry group. +Significant difference from pre approach (Two-way ANOVA), *Significant difference from saline (*t*-test), ˆSignificant difference from post-saline (Two-way ANOVA, Tukey's), $p \leqq 0.05$. . (For interpretation of the references to color in this figure legend, the reader is referred to the Web version of this article.)

(the gene name for CGRP) female and male mice were used. Mice received a unilateral injection of AAV9-hSyn-FLEX-jGCaMP7f-WPRE and a fiber optic implant in the BNST (Supplemental Fig. 1a), bilateral PBN injections of either CRE-dependent hM3D(G_q) DREADD (Fig. 2b) or CRE-dependent mCherry control virus (Fig. 2c). CNO (3 mg/kg, IP) or vehicle (saline) was administered 30-min prior to NSFT (Fig. 2a). Male and Female data was combined as no sex differences were observed.

During NSFT no significant effect of CNO was observed on total non-consummatory approach bouts (i.e., pellet not obtained) in the hM3D (G_q) (Fig. 2d, [$t_{31} = 0.4998$, $p = 0.6208$]) or mCherry groups (Fig. 2h, [$t_{31} = 0.7205$, $p = 0.4766$]). A clear BNST transient signal synchronized to the initiation of non-consummatory approach bouts emerged (Fig. 2e

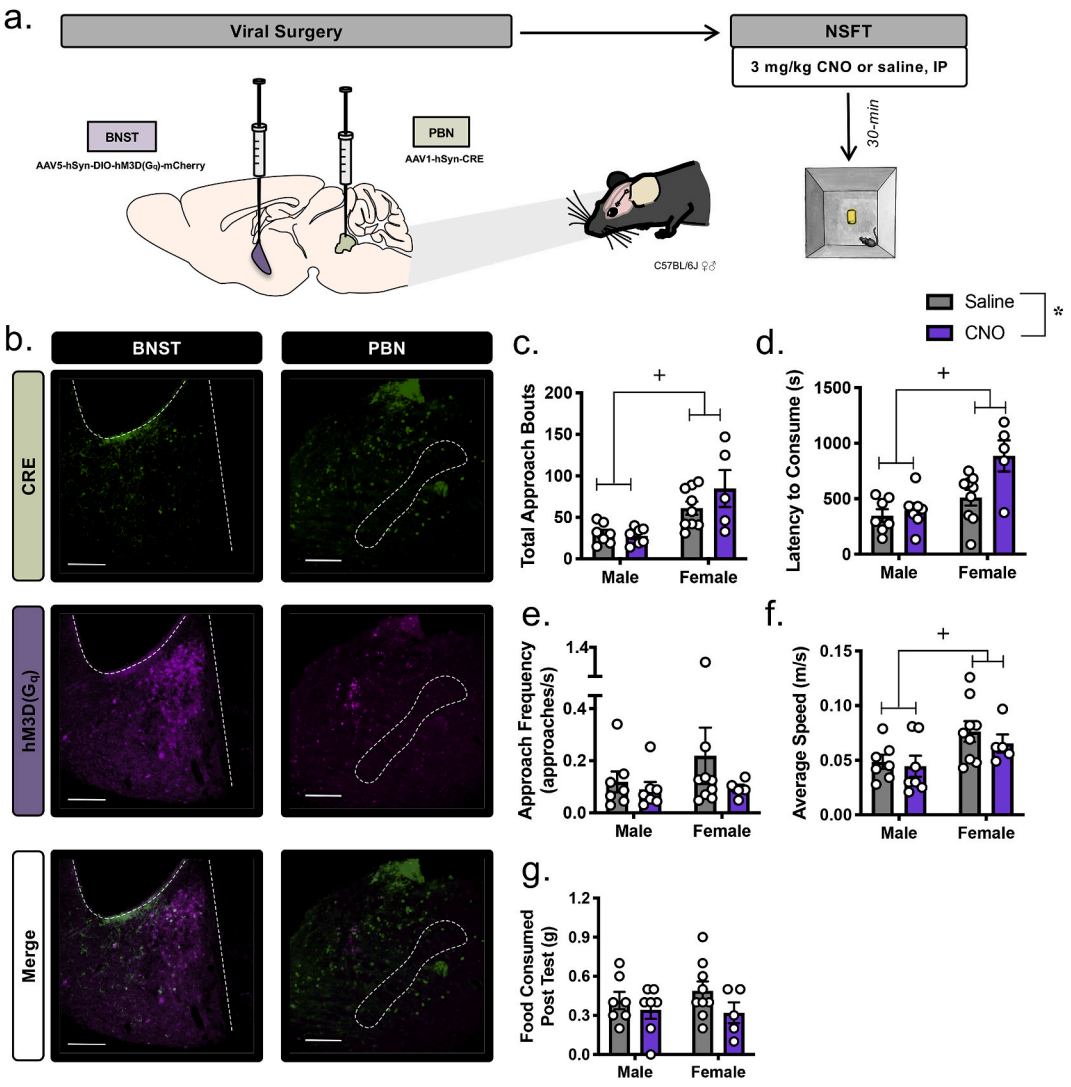

Fig. 3. Activation of BNST cells receiving PBN projections ($BNST^{PBN}$) differentially modulates latency to feed in males & females. **a)** Schematic demonstrating approach to selectively express hM3D(G_q) in BNST cells innervated by PBN projections ($BNST^{PBN}$) through bilateral infusion of the anterograde transsynaptic CRE in the PBN and bilateral infusions of the CRE-dependent hM3D(G_q) in the BNST of C57BL/6J female and male mice. **b)** Representative CRE, hM3D(G_q), and CRE + hM3D(G_q) merged immunofluorescence in the BNST (left column) and PBN (right column) **c)** Female mean ± S.E.M. total food approaches are increased relative to males ($p = 0.0002$). **d)** CNO treatment (3 mg/kg, IP) increased mean ± S.E.M. latency to consume center food in NSFT ($p = 0.0158$) with females exhibiting increased latency ($p = 0.0005$). **e)** Mean ± S.E.M. approach frequency, **f)** distance traveled during NSFT and **g)** total food consumed post-NSFT was similar in males and females with saline and CNO treatment. PBN Scale bar, 100 μm. BNST Scale bar, 200 μm +Significant difference from males (Two-way ANOVA), *Significant difference from saline (Two-way ANOVA), $p \leqq 0.05$.

and i) as demonstrated by a significant increase in amplitude in the hM3D(G_q) (Fig. 2f, main effect of time: [$F_{(1,600)} = 12.52$, $p = 0.0004$]) and mCherry group (Fig. 2j, main effect of time: [$F_{(1,600)} = 4.451$, $p = 0.0353$]) with Two-way ANOVA comparing area under the curve (AUC) pre-versus post-approach. AUC was analyzed to more accurately detect CNO-induced changes in amplitude of the BNST GCaMP7f signals. Two-way analysis of AUC indicates no main effect of treatment (hM3D(G_q), [$F_{(1,600)} = 0.04861$, $p = 0.8256$]; mCherry, [$F_{(1,600)} = 0.1455$, $p = 0.7030$]) nor significant time × treatment interaction (hM3D(G_q), [$F_{(1,600)} = 0.6632$, $p = 0.4158$]; mCherry, [$F_{(1,600)} = 0.5234$, $p = 0.4697$]) on AUC pre versus post non-consummatory approach bouts in the hM3D(G_q) (Fig. 2f) and mCherry (Fig. 2j) groups. Total AUC was also analyzed to capture CNO-induced changes throughout the initiation of non-consummatory approach bouts. AUC of the BNST GCaMP7f signal throughout non-consummatory approach bouts is similar with saline and CNO treatment in the hM3D(G_q) (Fig. 2g, [$t_{600} = 0.5202$ $p = 0.6031$]) and mCherry group (Fig. 2k, [$t_{600} = 1.132$ $p = 0.2580$]). Thus, hM3D(G_q) activation in PBN CGRP neurons did not affect total food approaches nor the synchronized BNST GCaMP transient at the time of non-consummatory approaches.

PBN CGRP neuron hM3D(G_q) activation by CNO significantly increased the average latency to feed (Fig. 2l, [$t_{31} = 3.081$, $p = 0.0043$]) but had no effect in the mCherry controls (Fig. 2p, [$t_{31} = 0.9605$, $p = 0.3442$]). A BNST transient signal synchronized to the time of the consummatory food approach emerged (Fig. 2m and q) as demonstrated by a significant increase in amplitude in the hM3D(G_q) (Fig. 2n, main effect of time: [$F_{(1,600)} = 144.0$, $p < 0.0001$]) and mCherry groups (Fig. 2r, main effect of time: $F_{(1,600)} = 92.44$, $p < 0.0001$) with Two-way ANOVA comparing AUC before versus after the consummatory approach. Additionally in the hM3D(G_q) group the Two-way ANOVA reveals a significant time × treatment interaction ($F_{(1,600)} = 10.47$, $p = 0.0013$) and a significant main effect of treatment ($F_{(1,600)} = 16.17$, $p < 0.0001$) indicating PBN CGRP neuron activation potentiated the amplitude of the BNST transient after the time of the consummatory food approach (Fig. 2n). In the mCherry group the Two-way ANOVA shows a significant time × treatment interaction ($F_{(1,600)} = 5.539$, $p =$

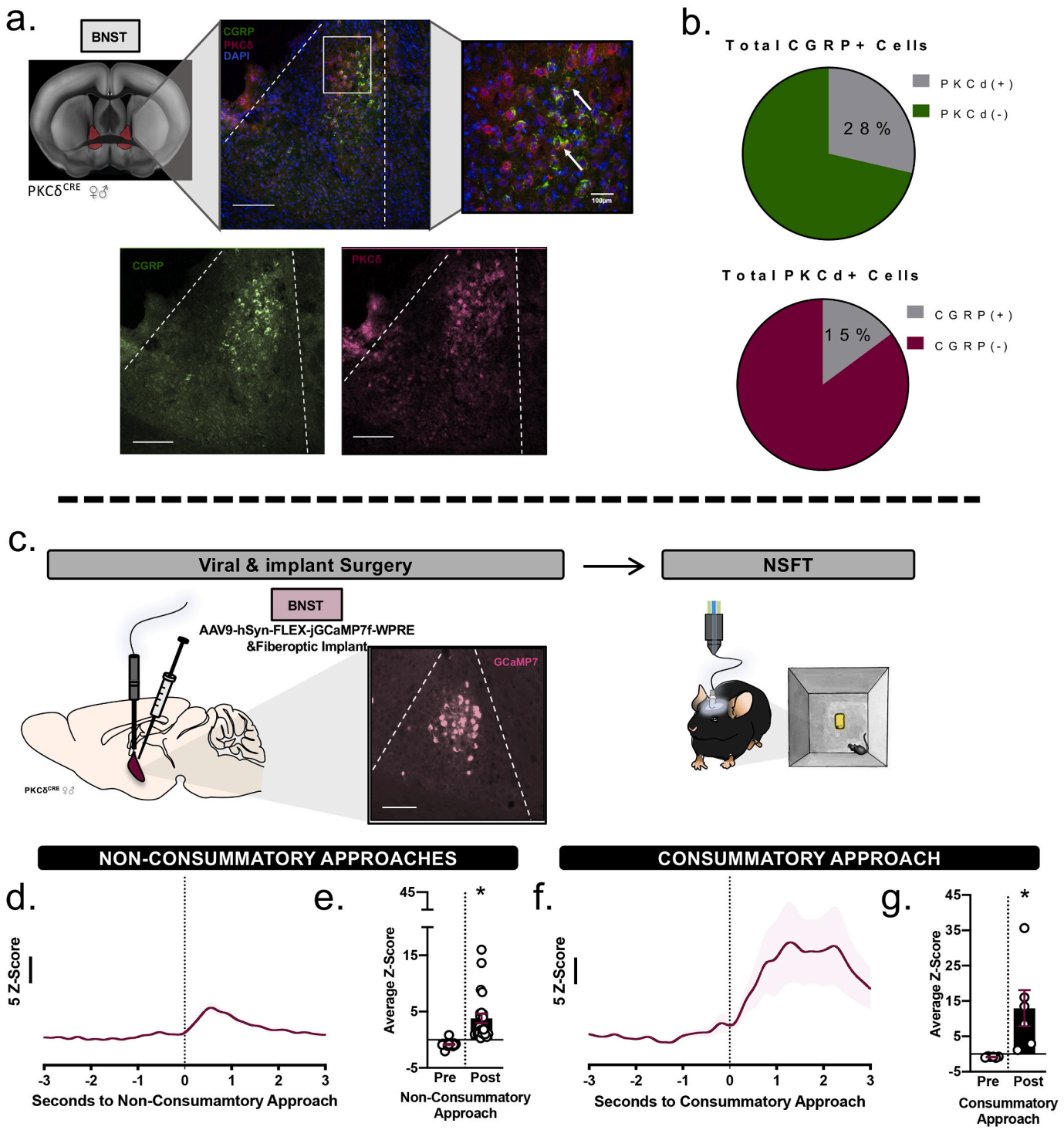

Fig. 4. PBN innervates PKCδ-specific BNST neurons and PKCδ GCaMP transients emerge at the time of food approach in NSFT **a)** Representative image demonstrating CGRP, PKCδ, and PKCδ+CGRP + DAPI merged immunofluorescence in the BNST **b**) Quantification of CGRP and PKCδ demonstrate PKCδ+CGRP colocalization, non-PKCδ and non-CGRP expressing cells in the BNST. **c)** Schematic demonstrating unilateral CRE-dependent GCaMP7f infusion & fiber optic implantation in the BNST of PKCδ^{CRE} female and male mice followed by testing with NSFT. **d)** Mean ± S.E.M of BNST GCaMP6f Z-Scores at the time of non-consummatory food approaches shows a transient signal. **e)** Mean ± S.E.M of the individual GCaMP6f Z-Score averages is significantly increased post a non-consummatory approach ($p < 0.0001$). **f)** Mean ± S.E.M of BNST GCaMP6f Z-Scores at the time of the consummatory approach shows a transient signal. **g)** Mean ± S.E.M of individual GCaMP6f Z-Score averages is significantly increased post the time of the consummatory approach ($p = 0.0015$). Scale bar, 200 μm and merged image: 100 μm *Significant from pre approach (paired *t*-test), $p \leqq 0.05$.

0.0189) and no main effect of treatment ($F_{(1,600)} = 1.302$, $p = 0.2542$) before versus after the time of the consummatory food approach (Fig. 2r). Further analysis of AUC of the BNST GCaMP7f signal throughout the consummatory approach reveals a significant effect of CNO treatment in the hM3D(G$_q$) group (Fig. 2o, [$t_{600} = 7.886$, $p < 0.0001$]). No effect of CNO on total AUC was detected throughout the consummatory approach in the mCherry group (Fig. 2s, [$t_{600} = 1.413$, $p = 0.1581$]).

Comparison of the behavioral data during NSFT demonstrates a significant decrease in the rate of approach bouts with PBN activation in the hM3D(G_q) (Fig. 2t, [$t_{31} = 2.381$, $p = 0.0236$]) but not the mCherry group (Fig. 2y, [$t_{31} = 0.7205$, $p = 0.4766$). There was no effect on average speed during NSFT nor average food consumed post-test in both hM3D(G_q) (Fig. 2u, [$t_{31} = 0.3834$, $p = 0.8842$]; Fig. 2v, [$t_{31} = 0.9293$, $p = 0.3599$]) and mCherry groups (Fig. 2z, [$t_{31} = 0.04193$, $p = 0.9668$]; Fig. 2aa, [$t_{31} = 0.3054$, $p = 0.7627$]). As an additional measure of physiological and psychological affect we recorded ultrasonic vocalizations (USVs) during NSFT, as changes in USV frequency measure changes in internal state (Arriaga and Jarvis, 2013; Coffey et al., 2019; Grimsley et al., 2016; Mun et al., 2015). The USVs detected demonstrated a significant decrease in average USV kHz frequency (Fig. 2w and x, [$t_8 = 3.406$, $p = 0.0093$]) in the hM3D(G_q) but not the mCherry group (Fig. 2ab and 2ac [$t_{10} = 0.6153$, $p = 0.5521$]). Together the data demonstrate hM3D(G_q) activation of PBN CGRP neurons increased the frequency of non-consummatory approach bouts, decreased the frequency of USVs, and increased the latency to feed synchronized to a potentiated phasic BNST GCaMP transient signal at the time of the consummatory approach.

3.3. Experiment 3: activation of $BNST^{PBN}$ delays NSFT consummatory approach behavior

To investigate the specific role PBN innervated BNST cells ($BNST^{PBN}$) play in modulating NSFT behavior, we utilized a novel anterograde transsynaptic viral transfer strategy (Centanni et al., 2019; Zingg et al., 2017; Zingg et al., 2020) allowing for specific manipulation of PBN-innervated BNST cells during NSFT (Fig. 3a). C57BL/6J male and female mice received bilateral injections of the transsynaptic AAV1-CRE in the PBN and CRE-dependent hM3D(G_q) DREADDs in the BNST (Fig. 3a and b), no differences in male and female expression were evident. Given that CNO had no effect in the mCherry control group in Experiment 2 and our previous study demonstrating the fidelity of AAV1 (Centanni et al., 2019) we did not include DREADD controls in this experiment. To selectively activate $BNST^{PBN}$, mice received CNO (3 mg/kg, IP) 30-min prior to NSFT (Fig. 3a). Two-way ANOVA, used to investigate potential sex differences, shows no significant sex × treatment interaction or treatment effect (Fig. 3c, [$F_{(1,24)} = 1.756$, $p = 0.1976$] [$F_{(1,24)} = 1.135$, $p = 0.2972$]) but there was a significant main effect of sex ($F_{(1,24)=}19.68$, $p = 0.0002$), suggesting an increase in food approach bouts in females. Two-way ANOVA comparing latency to feed shows a trend towards a sex × treatment interaction ($F_{(1,26)} = 4.053$, $p = 0.0554$), and reveals a main effect of sex ($F_{(1,24)} = 16.02$, $p = 0.0005$) and treatment ($F_{(1,24)} = 6.746$, $p = 0.0158$), thereby suggesting an increase in latency to feed in females and an increase following CNO treatment (Fig. 3d). There was no difference in frequency (Fig. 3e) as Two-way ANOVA demonstrates no significant main effect of sex ($F_{(1,24)} = 0.4511$, $p = 0.5315$), treatment ($F_{(1,24)} = 1.015$, $p = 0.5082$), nor sex × treatment interaction ($F_{(1,24)} = 0.4032$, $p = 0.5315$). Two-way ANOVA shows an increased speed (Fig. 3f) in females as there is a significant main effect of sex ($F_{(1,24)} = 7.061$, $p = 0.0138$) with no significant effect of treatment ($F_{(1,24)} = 0.6996$, $p = 0.4112$), nor sex × treatment interaction ($F_{(1,24)} = 0.1465$, $p = 0.7053$). There was no significant effect of sex ($F_{(1,24)} = 0.1120$, $p = 0.7299$), treatment ($F_{(1,24)} = 2.631$, $p = 0.1178$), nor sex × treatment interaction ($F_{(1,24)} = 0.4328$, $p = 0.5169$) on food consumption post-test (Fig. 3g). These data demonstrate that $BNST^{PBN}$ activation increased latency to feed in a sex-specific manner.

3.4. Experiment 4: phasic BNST PKCδ calcium signal associated with NSFT approach behavior

The data thus far suggest that PBN activation may in part drive the phasic bulk BNST transient signal at the time of food approach. Given the recently reported role of PKCδ-expressing cells in the BNST in food-related behaviors (Wang et al., 2019), and the stress-dependent alterations of expression of this kinase that we previously reported, we investigated whether PBN afferents synapsed on BNST(PKCδ) cells. The BNST of female and male $PKC\delta^{CRE}$ mice were analyzed for CGRP expression to identify PBN afferents and PKCδ expression in order to analyze colocalization of CGRP and PKCδ. Tissue analysis identified colocalization of CGRP innervated PKCδ cells in the BNST (Fig. 4a and b).

To investigate *in vivo* BNST(PKCδ) neuronal activity during an anxiety-like behavior, PKCδ-specific calcium was measured in the BNST during NSFT. $PKC\delta^{CRE}$ female and male mice received a unilateral injection of the calcium indicator GCaMP7f and were implanted with a fiber optic in the BNST as represented in Fig. 4c. Following recovery from surgery, BNST(PKCδ) calcium activity was recorded (Supplemental Fig. 1b) during NSFT (Fig. 4c). A clear BNST(PKCδ) transient signal was observed in both non-consummatory approaches (Fig. 4d) and the consummatory approach (Fig. 4f) demonstrated by a significant increase in amplitude measured by average Z-Score pre-versus post-non-consummatory approaches (Fig. 4e, [$t_{23} = 5.374$, $p < 0.0001$]) and the consummatory approach (Fig. 4g, [$t_5 = 2.663$, $p = 0.0447$]). These data reveal phasic BNST(PKCδ) GCaMP transients at the time of food approach. Moreover, given that the PBN innervates BNST(PKCδ) cells and modulates global BNST transients these data suggest a role of PBN to BNST(PKCδ) cells in modulating consummatory approach behavior.

4. Discussion

Circuits containing the BNST are implicated in negative-affect and stress responses, but patterns of *in vivo* activity of BNST neurons in approach-avoidance contexts are vastly unexplored. The data we report here using the novelty-suppressed feeding task (NSFT) demonstrate BNST phasic activity time-locked to the time of an object approach in an open space. To begin to explore presynaptic mechanisms driving BNST activity in NSFT, we investigated the role of PBN neurons and show a PBN-induced decrease in the frequency of non-consummatory food approaches. Additionally, PBN activation delayed the initiation of the consummatory approach behavior while simultaneously amplifying BNST phasic activity *in vivo*. Next, by investigating the PBN→BNST neurocircuitry at a postsynaptic level, we reveal chemogenetic activation of $BNST^{PBN}$ neurons potentially delayed the initiation of the consummatory approach in females but not males. Lastly, through cell-specific transgenic mice we provide anatomical evidence of PBN innervation of BNST(PKCδ) neurons and also demonstrate BNST(PKCδ) phasic activity at to the time of food approaches.

Our rudimentary knowledge of approach behavior in a stress-like state is based on presenting stimuli that recruit two competing impulses which in turn induce a continuous anxiety-like state until a behavior diminishes or removes the presence of one of the stimuli (Corr, 2013; Craig, 1917; Kirlic et al., 2017). Previous studies highlighted a role for the BNST in contexts requiring a behavioral response to an approach-avoidance situation (Centanni et al., 2019; Walker et al., 2003), but to date no study has assessed the dynamic patterns of *in vivo* BNST activity in such tasks. While recent technological advances in the detection of neuronal activity *in vivo* show transient and prolonged effects on BNST activity during avoidance of a predatory threat or an open space (Bjorni et al., 2020; Giardino et al., 2018; Harris et al., 2018), we are the first to reveal BNST transients temporarily synchronized to food and object approaches in a stress-inducing context. Despite behavioral differences in approach frequency, the BNST transient was evident at the time of all approaches regardless of food location and object, suggesting a role for the BNST in primarily signaling stress-inducing contexts. Based on the literature (Lebow and Chen, 2016) and these data we hypothesize that a stress-inducing context is sufficient to produce changes in BNST activity during object approach regardless of differences in overall anxiety-like state. Additional NSFT modifications will help delineate the stress and context specificity of BNST neuronal activity during approach.

Furthermore, the BNST consists of various cell-types with differing afferents, efferents, and patterns of activity in response to stress-like states (Lebow and Chen, 2016) thereby our bulk BNST signal encompasses activity across a wide population of neurons. Here we utilized a transgenic mouse line to reveal BNST(PKCδ) phasic neuronal activity at the time of food approaches which resembles bulk BNST activity and amplified activity during the consummatory approach, which further supports the proposed role of BNST(PKCδ) in feeding (Wang et al., 2019). The amplified BNST(PKCδ) signal provides a more synchronized response due to increased uniformity in the BNST(PKCδ) population which may drive the bulk BNST signal during non-consummatory approach either directly or by regulating other local BNST neuronal populations, a hypothesis that remains to be tested. In addition to the implicated role of longer-lasting and slower-onset of BNST activity in stress-inducing contexts, the present data captures the phasic and temporally-synchronized nature of bulk BNST and PKCδ-specific transient activity thereby implicating a more dynamic role for the BNST in stress.

The BNST integrates information to process responses to stress in part by incoming projections from the midbrain regions such as the PBN which is implicated in processing alert responses to ensure a safety state (Chiang et al., 2019; Palmiter, 2018). Previous literature on CGRP-expressing PBN projections to the BNST set forth an excitatory role for the circuit in establishing and maintaining conditioned taste aversion to novel food and other consummatory behaviors in a disease-like state (Carter et al., 2013; Chen et al., 2018). However, studies using open field and elevated plus maze established that PBN activation only induced an anxiogenic phenotype under a state of malaise (Campos et al., 2017). Now we provide evidence that in a basal non-noxious state, global PBN and $BNST^{PBN}$ activation induced anxiety-like behavior and had no effect on food intake post-NSFT. Additionally, we demonstrate that PBN activation decreased the kHz frequency of the rodent-emitted USVs during NSFT. Given that USVs at frequencies above 40-kHz are associated with positive states and frequencies below 40-kHz are associated with stress-inducing states and contexts (Coffey et al., 2019; Grimsley et al., 2016; Mun et al., 2015), this data further supports a role for the PBN (Arriaga and Jarvis, 2013) in modulating negative psychological and physiological affective states. Thereby our data imply that PBN→BNST circuitry modulates a differing aspect of approach-related behavior under a non-noxious state as it delayed the time in which avoidance of the center in an unpredictable context was overcome by the consummatory approach behavior. Global PBN activation, but not specific activation of PBN→BNST, increased frequency of approach bouts, suggesting that active avoidance is not mediated through $BNST^{PBN}$ and thereby may be induced by other PBN efferent projections such as the central amygdala (CeA; (Cai et al., 2014; Carter et al., 2013). These data imply that the PBN→BNST circuit may in part delay the final behavioral response to a food vs safety situation.

Interestingly, the data suggest the increase in anxiety-like behavior following $BNST^{PBN}$ activation was only in females. To our knowledge our findings are the first to suggest a sex-specific effect within the PBN→BNST circuit. The BNST is a sexually dimorphic region with structural and cellular heterogeneity between males and females. This is demonstrated through clinical and preclinical studies, the latter of which highlight a particular role for PKCδ-expressing neurons in females (Fetterly et al., 2019). Given that we and others demonstrate anatomical innervation by the PBN onto BNST(PKCδ) cells (Wang et al., 2019) and that the BNST(PKCδ) activity displayed a similar phasic pattern as bulk BNST activity, the data warrants further investigation of PBN-induced BNST(PKCδ) activity and behavior. There is extensive literature of PBN to CeA PKCδ-specific interactions on modulating behavior particularly with fear conditioning and food-related avoidance (Cai et al., 2014; Carter et al., 2013; Chiang et al., 2019; Palmiter, 2018) and anatomical studies demonstrate collateral PBN projections to BNST and amygdala (Ye and Veinante, 2019). Thus, our studies may in part recruit the PBN→CeA circuitry. It will be important for future studies to dissect the differing or contributing roles of the PBN to BNST and PBN to CeA circuits (Lebow and Chen, 2016). Furthermore, given that the majority of PBN to CeA studies target CGRP-expressing projections, our $BNST^{PBN}$ manipulations were not on a transgenic background (albeit all other PBN manipulations were CGRP-specific) the transgenic differences within our study may account for the sex-specific effect. Non-CGRP expressing PBN projections also project to the BNST and can release glutamate and a combination of neuropeptides (Ye and Veinante, 2019). Future studies will need to investigate the role of non-CGRP expressing PBN projections particularly since *ex vivo* electrophysiological studies demonstrate differences in PBN to BNST projection kinetics (Flavin et al., 2014). Additionally, the BNST and PBN share reciprocal projections, hence we cannot conclusively say that our viral studies did not recruit BNST to PBN projections through retrograde transmission and in turn contribute to the observed anxiety-like behavior. Thus, it will be important for future studies to investigate how the PBN to BNST projections modulate other BNST and PBN neurocircuitry.

Our data demonstrating bulk and PKCδ-specific BNST transients during all object approaches in NSFT are consistent with the view that the BNST functions as a reward-avoidance integrator, processing opposing hedonic states to influence responses to stress (Park et al., 2012). Additionally, our data support a role of the PBN neurocircuitry in safety processing and suggest a role in modulating anxiety-like behavior in a non-noxious and non-aversive state.

5. Conclusions

Neurocognitive literature provides a framework for human behavior in stress-inducing approach-avoidance situations and defines the final behavior as the conflict resolution (Barker et al., 2019), which is shown to be driven in part by the BNST (Corr, 2013; Cryan and Sweeney, 2011; Kirlic et al., 2017). Our preclinical study is complimentary to this framework and suggests that the PBN drives BNST activity during behavior resulting in conflict resolution, potentially in a sex-specific manner. Given the need for effective treatments to alleviate maladaptive behavioral responses to stress and the relevance of anxiety in females these data strongly suggest the PBN→BNST is a component of the approach circuitry that needs to be targeted and further studied.

Funding

This work was supported by the National Institutes of Health NIAAA Diversity Supplement AA019455-09S1 (AAJ) and other grants from NIAAA AA019455 (DGW), NIDA DA042475 (DGW), and Brain and Behavior Research Foundation NARSAD 27172 (SWC). Imaging was performed in part through the use of the Vanderbilt University School of Medicine Cell Imaging Shared Resource (supported by National Institutes of Health Grants CA68485, DK20593, DK58404, DK59637, and EY08126). Behavioral testing was performed in part through the Vanderbilt Neurobehavioral Core.

CRediT authorship contribution statement

A.A. Jaramillo: Project administration, Conceptualization, Investigation, Visualization, Writing - original draft. **K.M. Williford:** Investigation, Visualization, Writing - review & editing. **C. Marshall:** Investigation. **D.G. Winder:** Supervision, Conceptualization, Writing - review & editing. **S.W. Centanni:** Supervision, Conceptualization, Software, Investigation, Visualization, Writing - review & editing.

Declaration of competing interest

None.

Acknowledgements

We thank Richard Palmiter, Ph.D., for providing the *Calca*^{CRE} transgenic mouse line, and for comments on a previous version of this manuscript (University of Washington). We would like to thank Elana Milano, Bob Matthews, Ph.D., and John Allison, Ph.D. for technical assistance. Graphics provided by Katie Holleran, Ph.D., Rafael Perez, Ph. D., and Gregory J. Salimando, Ph.D.

Appendix A. Supplementary data

Supplementary data to this article can be found online at https://doi.org/10.1016/j.ynstr.2020.100247.

References

Adhikari, A., 2014. Distributed circuits underlying anxiety. Front. Behav. Neurosci. 8, 112.
Arriaga, G., Jarvis, E.D., 2013. Mouse vocal communication system: are ultrasounds learned or innate? Brain Lang. 124, 96–116.
Avery, S.N., Clauss, J.A., Blackford, J.U., 2016. The human BNST: functional role in anxiety and addiction. Neuropsychopharmacology 41, 126–141.
Avery, S.N., Clauss, J.A., Winder, D.G., Woodward, N., Heckers, S., Blackford, J.U., 2014. BNST neurocircuitry in humans. Neuroimage 91, 311–323.
Barker, T.V., Buzzell, G.A., Fox, N.A., 2019. Approach, avoidance, and the detection of conflict in the development of behavioral inhibition. New Ideas Psychol. 53, 2–12.
Bjorni, M., Rovero, N.G., Yang, E.R., Holmes, A., Halladay, L.R., 2020. Phasic signaling in the bed nucleus of the stria terminalis during fear learning predicts within- and across-session cued fear expression. Learn. Mem. 27, 83–90.
Bodnoff, S.R., Suranyi-Cadotte, B., Aitken, D.H., Quirion, R., Meaney, M.J., 1988. The effects of chronic antidepressant treatment in an animal model of anxiety. Psychopharmacology (Berlin) 95, 298–302.
Britton, D.R., Britton, K.T., 1981. A sensitive open field measure of anxiolytic drug activity. Pharmacol. Biochem. Behav. 15, 577–582.
Cai, H., Haubensak, W., Anthony, T.E., Anderson, D.J., 2014. Central amygdala PKC-delta(+) neurons mediate the influence of multiple anorexigenic signals. Nat. Neurosci. 17, 1240–1248.
Campos, C.A., Bowen, A.J., Han, S., Wisse, B.E., Palmiter, R.D., Schwartz, M.W., 2017. Cancer-induced anorexia and malaise are mediated by CGRP neurons in the parabrachial nucleus. Nat. Neurosci. 20, 934–942.
Carter, M.E., Soden, M.E., Zweifel, L.S., Palmiter, R.D., 2013. Genetic identification of a neural circuit that suppresses appetite. Nature 503, 111–114.
Centanni, S.W., Morris, B.D., Luchsinger, J.R., Bedse, G., Fetterly, T.L., Patel, S., et al., 2019. Endocannabinoid control of the insular-bed nucleus of the stria terminalis circuit regulates negative affective behavior associated with alcohol abstinence. Neuropsychopharmacology 44, 526–537.
Chen, J.Y., Campos, C.A., Jarvie, B.C., Palmiter, R.D., 2018. Parabrachial CGRP neurons establish and sustain aversive taste memories. Neuron 100, 891–899 e5.
Chiang, M.C., Bowen, A., Schier, L.A., Tupone, D., Uddin, O., Heinricher, M.M., 2019. Parabrachial complex: a hub for pain and aversion. J. Neurosci. 39, 8225–8230.
Coffey, K.R., Marx, R.G., Neumaier, J.F., 2019. DeepSqueak: a deep learning-based system for detection and analysis of ultrasonic vocalizations. Neuropsychopharmacology 44, 859–868.
Corr, P.J., 2013. Approach and avoidance behaviour: multiple systems and their interactions. Emotion Review 5, 285–290.
Craig, W., 1917. Appetites and aversions as constituents of instincts. Proc. Natl. Acad. Sci. U. S. A. 3, 685–688.
Cryan, J.F., Sweeney, F.F., 2011. The age of anxiety: role of animal models of anxiolytic action in drug discovery. Br. J. Pharmacol. 164, 1129–1161.
Cui, G., Jun, S.B., Jin, X., Luo, G., Pham, M.D., Lovinger, D.M., et al., 2014. Deep brain optical measurements of cell type-specific neural activity in behaving mice. Nat. Protoc. 9, 1213–1228.
Dong, H.W., Petrovich, G.D., Watts, A.G., Swanson, L.W., 2001. Basic organization of projections from the oval and fusiform nuclei of the bed nuclei of the stria terminalis in adult rat brain. J. Comp. Neurol. 436, 430–455.
Fetterly, T.L., Basu, A., Nabit, B.P., Awad, E., Williford, K.M., Centanni, S.W., et al., 2019. alpha2A-Adrenergic receptor activation decreases parabrachial nucleus excitatory drive onto BNST CRF neurons and reduces their activity in vivo. J. Neurosci. 39, 472–484.
Flavin, S.A., Matthews, R.T., Wang, Q., Muly, E.C., Winder, D.G., 2014. alpha(2A)-adrenergic receptors filter parabrachial inputs to the bed nucleus of the stria terminalis. J. Neurosci. 34, 9319–9331.
Flook, E.A., Feola, B., Avery, S.N., Winder, D.G., Woodward, N.D., Heckers, S., Blackford, J.U., 2020. BNST-insula structural connectivity in humans. Neuroimage 210, 116555.
Giardino, W.J., Eban-Rothschild, A., Christoffel, D.J., Li, S.B., Malenka, R.C., De Lecea, L., 2018. Parallel circuits from the bed nuclei of stria terminalis to the lateral hypothalamus drive opposing emotional states. Nat. Neurosci. 21, 1084–1095.
Goode, T.D., Maren, S., 2017. Role of the bed nucleus of the stria terminalis in aversive learning and memory. Learn. Mem. 24, 480–491.
Grimsley, J.M., Sheth, S., Vallabh, N., Grimsley, C.A., Bhattal, J., Latsko, M., et al., 2016. Contextual modulation of vocal behavior in mouse: newly identified 12 kHz "Mid-Frequency" vocalization emitted during restraint. Front. Behav. Neurosci. 10, 38.
Harris, N.A., Isaac, A.T., Gunther, A., Merkel, K., Melchior, J., Xu, M., et al., 2018. Dorsal BNST alpha2A-adrenergic receptors produce HCN-dependent excitatory actions that initiate anxiogenic behaviors. J. Neurosci. 38, 8922–8942.
Holleran, K.M., Wilson, H.H., Fetterly, T.L., Bluett, R.J., Centanni, S.W., Gilfarb, R.A., et al., 2016. Ketamine and MAG lipase inhibitor-dependent reversal of evolving depressive-like behavior during forced abstinence from alcohol drinking. Neuropsychopharmacology 41, 2062–2071.
Kirlic, N., Young, J., Aupperle, R.L., 2017. Animal to human translational paradigms relevant for approach avoidance conflict decision making. Behav. Res. Ther. 96, 14–29.
Lebow, M.A., Chen, A., 2016. Overshadowed by the amygdala: the bed nucleus of the stria terminalis emerges as key to psychiatric disorders. Mol. Psychiatr. 21, 450–463.
Mccoy, E.S., Taylor-Blake, B., Street, S.E., Pribisko, A.L., Zheng, J., Zylka, M.J., 2013. Peptidergic CGRPalpha primary sensory neurons encode heat and itch and tonically suppress sensitivity to cold. Neuron 78, 138–151.
Miller, N.E., 1944. Experimental Studies of Conflict. Ronald Press.
Mun, H.S., Lipina, T.V., Roder, J.C., 2015. Ultrasonic vocalizations in mice during exploratory behavior are context-dependent. Front. Behav. Neurosci. 9, 316.
Novais, A., Monteiro, S., Roque, S., Correia-Neves, M., Sousa, N., 2017. How age, sex and genotype shape the stress response. Neurobiol Stress 6, 44–56.
Palmiter, R.D., 2018. The parabrachial nucleus: CGRP neurons function as a general alarm. Trends Neurosci. 41, 280–293.
Park, J., Wheeler, R.A., Fontillas, K., Keithley, R.B., Carelli, R.M., Wightman, R.M., 2012. Catecholamines in the bed nucleus of the stria terminalis reciprocally respond to reward and aversion. Biol. Psychiatr. 71, 327–334.
Shin, L.M., Liberzon, I., 2010. The neurocircuitry of fear, stress, and anxiety disorders. Neuropsychopharmacology 35, 169–191.
Walker, D.L., Toufexis, D.J., Davis, M., 2003. Role of the bed nucleus of the stria terminalis versus the amygdala in fear, stress, and anxiety. Eur. J. Pharmacol. 463, 199–216.
Wang, Y., Kim, J., Schmit, M.B., Cho, T.S., Fang, C., Cai, H., 2019. A bed nucleus of stria terminalis microcircuit regulating inflammation-associated modulation of feeding. Nat. Commun. 10, 2769.
Wenzel, J.M., Waldroup, S.A., Haber, Z.M., Su, Z.I., Ben-Shahar, O., Ettenberg, A., 2011. Effects of lidocaine-induced inactivation of the bed nucleus of the stria terminalis, the central or the basolateral nucleus of the amygdala on the opponent-process actions of self-administered cocaine in rats. Psychopharmacology (Berlin) 217, 221–230.
Ye, J., Veinante, P., 2019. Cell-type specific parallel circuits in the bed nucleus of the stria terminalis and the central nucleus of the amygdala of the mouse. Brain Struct. Funct. 224, 1067–1095.
Zingg, B., Chou, X.L., Zhang, Z.G., Mesik, L., Liang, F., Tao, H.W., et al., 2017. AAV-mediated anterograde transsynaptic tagging: mapping corticocollicular input-defined neural pathways for defense behaviors. Neuron 93, 33–47.
Zingg, B., Peng, B., Huang, J., Tao, H.W., Zhang, L.I., 2020. Synaptic specificity and application of anterograde trans-synaptic AAV for probing neural circuitry. J. Neurosci. 40, 3250–3267.